JETIR.ORG ISSN: 2349-5162 | ESTD Year : 2014 | Monthly Issue
JOURNAL OF EMERGING TECHNOLOGIES AND INNOVATIVE RESEARCH (JETIR)
An International Scholarly Open Access, Peer-reviewed, Refereed Journal

PHOTOLUMINESCENCE BEHAVIOR OF CE^{3+}, EU^{3+}, AND DY^{3+} DOPED PHOSPHATE-BASED NANOPHOSPHORS FOR OPTOELECTRONIC APPLICATIONS

Roshni Haldkar*[1] R.K. Kuraria*[2] Shashi R. Kuraria*[3] Anjali Yadav*[4]

*[1,*3,*4]Govt. Science College, Jabalpur(M.P.) 482001, India,

*[2]Vice chancellor Awdhesh Pratap Singh University (APSU) Rewa, Madhya Pradesh, 486002, India

Abstract:In this study, the photoluminescence properties of rare-earth doped phosphate-based nanophosphors were investigated, focusing on Ce^{3+}, Eu^{3+}, and Dy^{3+} ions incorporated into $Mg_4P_2O_7$, $Ca_4P_2O_7$, and $Sr_4P_2O_7$ host lattices. Photoluminescence spectra revealed sharp excitation and emission peaks corresponding to the characteristic f–f and f–d transitions of rare-earth ions. $Mg_4P_2O_7$:Eu^{3+} and $Sr_4P_2O_7$:Eu^{3+} exhibited strong red emissions around 615 nm and 612 nm, respectively, under near-UV excitation. Ce^{3+} doped systems displayed intense green luminescence, while Dy^{3+} doped $Sr_4P_2O_7$ phosphors showed a combination of blue, yellow, and red emissions, suggesting their potential for white-light emission. Optimal doping concentrations were identified for maximum emission intensity, beyond which concentration quenching was observed. These findings highlight the tunable optical properties of rare-earth doped pyrophosphate phosphors and their suitability for solid-state lighting and display technologies.

***Keywords*- Photoluminescence, Phosphate-based nano phosphors, Application.**

I. INTRODUCTION

In recent decades, the development of efficient and stable luminescent materials has garnered immense attention due to their widespread applications in solid-state lighting, display technologies, biological imaging, and optical thermometry. Among the various luminescent materials, rare-earth doped phosphors have emerged as a prominent class of compounds owing to their sharp emission lines, excellent thermal and chemical stability, and high quantum efficiency. Europium (Eu^{3+}), in particular, has gained considerable interest as a red-emitting activator ion due to its intense and characteristic $^5D_0 \rightarrow {}^7F_j$ (J = 0–4) electronic transitions, making it highly desirable for applications in red-emitting phosphors**[1-5]**.

Magnesium pyrophosphate ($Mg_4P_2O_7$) has recently attracted attention as a promising host lattice for rare-earth doping due to its desirable properties such as high thermal stability, low phonon energy, and good chemical durability. The pyrophosphate ($P_2O_7^{4-}$) anion consists of a dimeric structure formed by two PO_4 tetrahedra sharing one oxygen atom, which provides a robust three-dimensional network capable of incorporating various rare-earth ions without significantly distorting the host lattice. Additionally, Mg^{2+} ions can be partially substituted with trivalent Eu^{3+} ions due to their comparable ionic radii, allowing for effective energy transfer and luminescence generation**[6-10]**.

The choice of $Mg_4P_2O_7$ as a host is further justified by its favorable band structure and the ability to form a crystalline phase at relatively lower temperatures compared to other phosphate-based matrices. The rigid lattice of pyrophosphate also helps suppress non-radiative relaxation processes, thereby enhancing the luminescent efficiency of the doped system. Despite these advantages, studies on Eu^{3+}-activated $Mg_4P_2O_7$ phosphors are relatively limited, and systematic investigations into the structural, vibrational, and luminescent properties of these materials are still needed**[11-15]**.

Therefore, in this study, we report the synthesis of Eu^{3+}-doped $Mg_4P_2O_7$ phosphors using a high-temperature solid-state reaction method. The structural and morphological characteristics of the prepared samples were thoroughly analyzed using X-ray diffraction (XRD), SEM, TEM, TGA and Fourier transform infrared (FT-IR) spectroscopy. Photoluminescence (PL) studies, including excitation and emission spectra, were carried out to evaluate the optical behavior of the Eu^{3+} activator in the host lattice. The effect of dopant concentration and calcination temperature on the crystallinity and luminescence properties was also explored. The results presented herein aim to provide valuable insight into the design of efficient red-emitting phosphors based on pyrophosphate hosts for potential use in advanced photonic applications.

II. Photoluminance properties

Photoluminance of $Mg_4P_2O_7:Eu^{+3}$

The photoluminescence properties of **$Mg_4P_2O_7:Eu^{3+}$** phosphor were evaluated through both excitation and emission spectra, providing insights into its optical behavior. The excitation spectrum (**Figure1a**), monitored at an emission wavelength of 593 nm, exhibits a broad and intense band centered at around 265 nm, which can be attributed to charge transfer transitions from the oxygen ligands to the Eu^{3+} ions. In addition to this broad band, several sharp peaks are observed at 319, 358, 393, and 395 nm, corresponding to the characteristic f–f transitions of Eu^{3+} ions, particularly the transitions from the ground state ($^7F_0$) to various excited states such as $^5H_4$, $^5D_4$, and $^5L_6$. Among them, the strong excitation peak at 395 nm indicates that the phosphor can be efficiently excited by near-UV light, making it compatible with commercially available near-UV LED chips.

The emission spectrum (**Figure 1 b**), recorded under 395 nm excitation, reveals multiple sharp emission peaks, which are characteristic of Eu^{3+} ion transitions. The most prominent emission peaks are observed at 593 nm, 615 nm, and 652 nm, which correspond to the $^5D_0 \rightarrow {}^7F_1$, $^5D_0 \rightarrow {}^7F_2$, and $^5D_0 \rightarrow {}^7F_3$ transitions, respectively. The intense red emission peak at 615 nm ($^5D_0 \rightarrow {}^7F_2$) signifies a strong electric dipole transition, indicating that Eu^{3+} ions occupy sites with non-centrosymmetric environments in the host lattice. The presence of the 593 nm peak ($^5D_0 \rightarrow {}^7F_1$), a magnetic dipole transition, further complements the emission profile, providing orange-red luminescence.

Overall, the excitation and emission analysis confirms that $Mg_4P_2O_7:Eu^{3+}$ is an efficient red-emitting phosphor with excellent potential for application in white light-emitting diodes (w-LEDs) and other optoelectronic devices that rely on rare-earth doped luminescent materials.

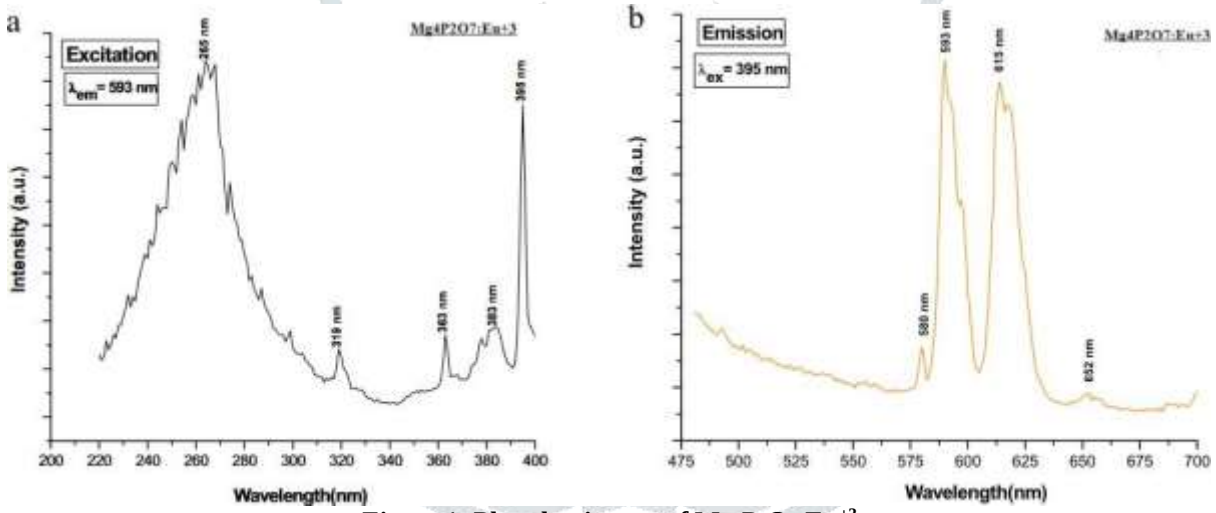

Figure 1: Photoluminance of $Mg_4P_2O_7:Eu^{+3}$

Photoluminance of $Mg_4P_2O_7:Ce^{+3}$

Figure 2a displays the photoluminescence excitation spectrum of $Mg_4P_2O_7$ doped with Ce^{3+} ions, monitored at an emission wavelength of 545 nm. The spectrum shows a broad excitation band centered around 240 nm, attributed to the charge transfer transition from the $4f^8$ ground state to the $4f^75d^1$ excited state of Ce^{3+}. This broad band is characteristic of the allowed 4f → 5d transitions in rare-earth ions and indicates that the optimal excitation wavelength lies in the UV region, making 245 nm an appropriate excitation source for studying the emission behavior of this phosphor.

Figure 2b shows the emission spectra of $Mg_4P_2O_7:Ce^{3+}$ phosphors under 245 nm excitation for varying Ce^{3+} concentrations (x = 0.01 to 0.06). The emission spectra consist of multiple peaks, with the most prominent emission occurring at ~545 nm, corresponding to the $^5D_4 \rightarrow {}^7F_5$ transition of Ce^{3+}. Other observed transitions include $^5D_4 \rightarrow {}^7F_6$ (490 nm), $^5D_4 \rightarrow {}^7F_4$ (585 nm), and $^5D_4 \rightarrow {}^7F_3$ (620 nm), all of which are typical for Ce^{3+} ions. The green emission (~545 nm) dominates, which is desirable for display and lighting applications.

The inset in **Figure 2b** illustrates the variation of emission intensity at 545 nm with increasing Ce^{3+} concentration. The intensity increases initially with increasing dopant concentration, reaching a maximum at x = 0.04. Beyond this concentration, the intensity starts to decrease, indicating the onset of concentration quenching. This suggests that energy transfer among Ce^{3+} ions becomes non-radiative at higher concentrations due to cross-relaxation processes or energy migration to quenching sites.

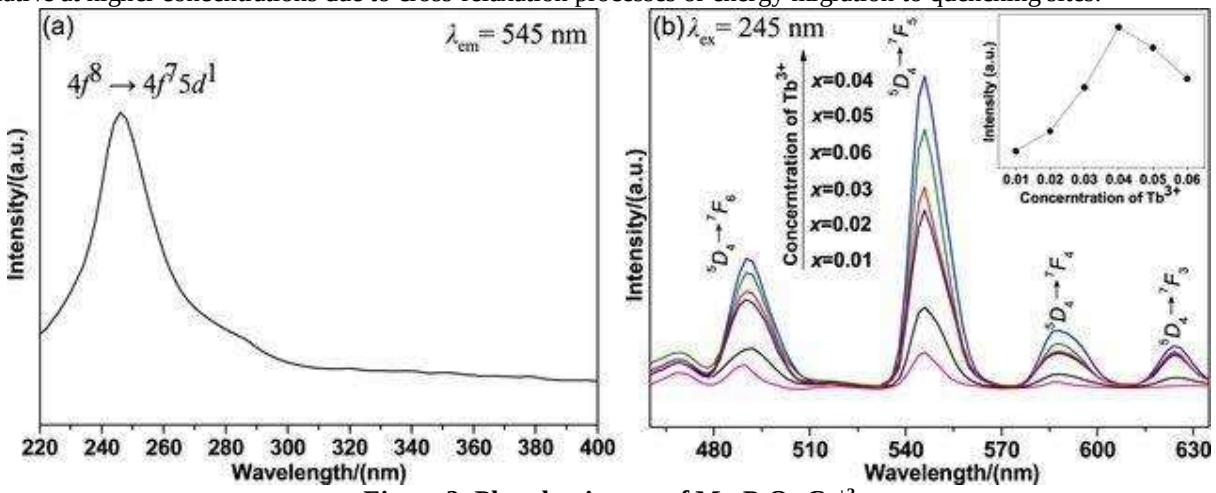

Figure 2: Photoluminance of $Mg_4P_2O_7:Ce^{+3}$

Photoluminance of $Ca_4P_2O_7:Eu^{+3}$

Figure 3 (a) presents the emission spectra of $Ca_4P_2O_7$ doped with varying concentrations of Eu^{3+} ions (x = 0.02 to 0.08), under excitation at 330 nm. A prominent emission peak is observed at around 422 nm, which corresponds to the electronic transition of Eu^{2+} ions from the $4f^65d^1$ excited state to the $4f^7$ ground state. This strong blue emission confirms that a fraction of Eu^{3+} ions are reduced to Eu^{2+} within the host lattice. The inset graph reveals that the emission intensity initially increases with Eu concentration and peaks at x = 0.06, beyond which concentration quenching reduces the intensity. Additionally, a slight red shift in emission wavelength is observed with increased Eu doping, likely due to the changes in crystal field environment.

Figure 3(b) shows the excitation spectra of $Ca_4P_2O_7:Eu^{2+}$ phosphors monitored at an emission wavelength of 422 nm. The spectra reveal broad excitation bands, with two dominant peaks centered around 288 nm and 330 nm. These bands are attributed to the allowed $4f^7 \rightarrow 4f^65d^1$ transitions of Eu^{2+} ions. The broadness of these excitation bands is a characteristic feature of the 5d levels in Eu^{2+}, which are highly sensitive to the surrounding crystal field. The increase in intensity with higher Eu^{2+} concentration (up to x = 0.08) suggests efficient absorption of UV light, though the saturation trend hints at an optimal doping limit for maximum excitation efficiency.

Both emission and excitation spectra indicate that the luminescence of $Ca_4P_2O_7:Eu^{2+}$ is highly dependent on the Eu^{2+} doping concentration. The optimal concentration is around x = 0.06, beyond which non-radiative energy transfer mechanisms likely dominate, resulting in emission quenching. The presence of both Eu^{3+} and Eu^{2+} emissions also implies that partial reduction occurs during synthesis, and the luminescent properties can be tuned by adjusting the Eu ion ratio and the synthesis atmosphere. Overall, $Ca_4P_2O_7:Eu^{2+}$ exhibits potential as an efficient blue-emitting phosphor under near-UV excitation.

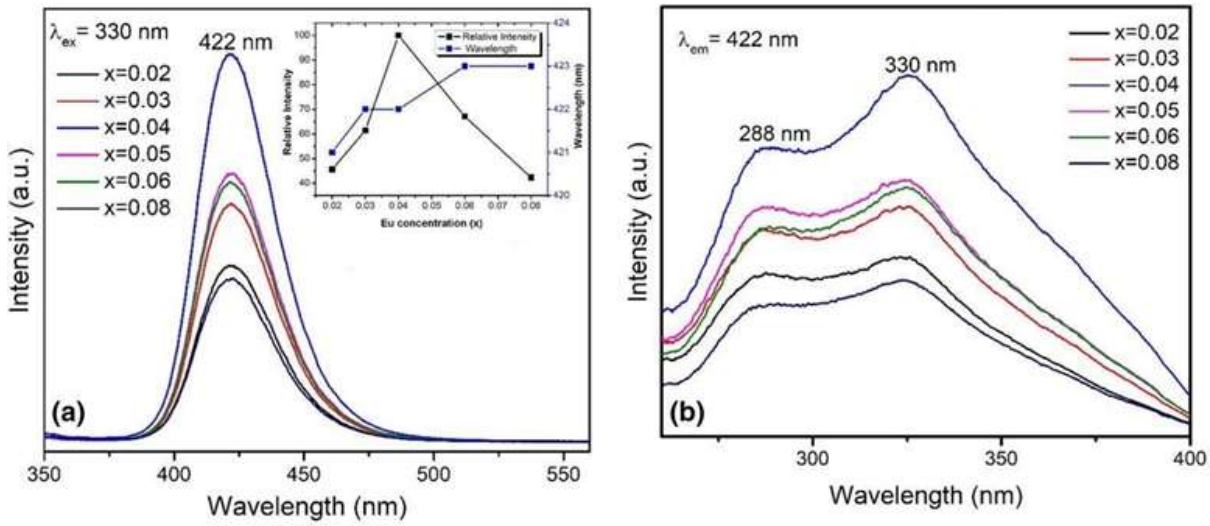

Figure 3: Photoluminance of $Ca_4P_2O_7:Eu^{+3}$

Photoluminescence (PL) of $Sr_4P_2O_7:Eu^{3+}$

The photoluminescence (PL) spectrum of $Sr_4P_2O_7:Eu^{3+}$ reveals a characteristic excitation band in the UV region, ranging from approximately 250 to 400 nm, with prominent peaks centered around 300–350 nm. This broad excitation band is attributed to the charge transfer transition from O^{2-} to Eu^{3+}, which is a common excitation mechanism in Eu^{3+}-doped phosphors. Upon excitation, the emission spectrum displays sharp and intense peaks in the visible region, particularly dominated by the prominent red emission at ~612 nm, which corresponds to the electric dipole transition $^5D_0 \rightarrow {}^7F_2$ of Eu^{3+}. This transition is hypersensitive to the local environment and suggests that Eu^{3+} ions occupy non-centrosymmetric sites in the $Sr_4P_2O_7$ host lattice. The presence of additional weaker emission lines corresponding to other $^5D_0 \rightarrow {}^7F_j$ transitions (j = 0, 1, 3, 4) further confirms the characteristic luminescent behavior of Eu^{3+}. Overall, the PL analysis indicates efficient UV-to-visible light conversion and strong red emission, making $Sr_4P_2O_7:Eu^{3+}$ a promising red-emitting phosphor for optical and display applications.

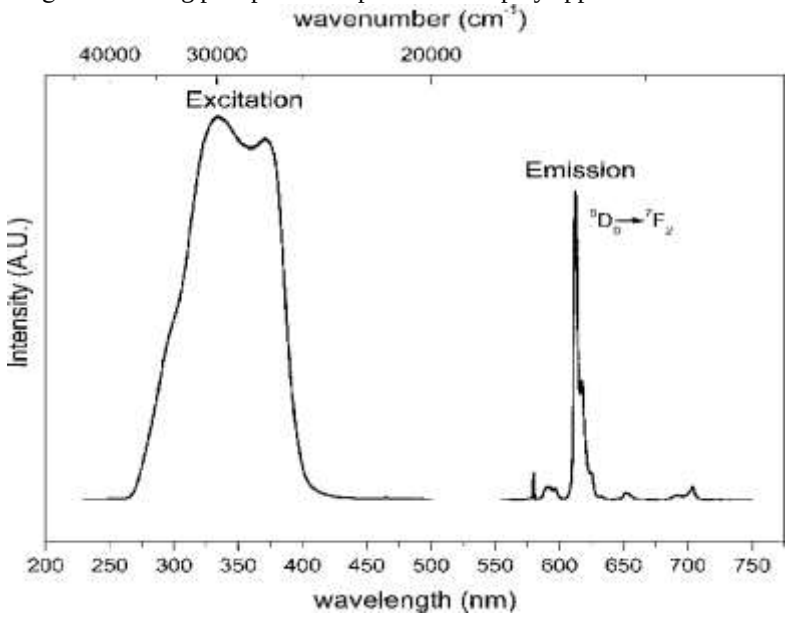

Figure 4: Photoluminescence (PL) of $Sr_4P_2O_7:Eu^{3+}$

Photoluminescence (PL) of $Sr_4P_2O_7:Ce^{3+}$

The photoluminescence (PL) spectra of $Sr_4P_2O_7:Ce^{3+}$ exhibit characteristic features of trivalent cerium ions, with excitation and emission behaviors captured in the two panels. In the upper panel, the red line shows the excitation spectrum monitored at an emission wavelength of 544.1 nm, revealing several prominent excitation bands in the UV region, notably peaking at 370 nm. The corresponding emission spectrum (black line) features multiple sharp peaks, particularly from ~400 to ~600 nm, which are attributed to the $5D_4 \rightarrow {}^7F_j$ transitions of Ce^{3+} ions, where j = 6, 5, 4, 3. These narrow lines indicate the f–f transitions typical for rare-earth ions in a crystalline host lattice.

In the lower panel, the excitation spectrum (red) is recorded at the emission wavelength of 658.0 nm and shows a strong absorption band centered at 362 nm. The corresponding emission spectrum (black line) displays peaks corresponding to transitions from the $^5F_5$ and $^5S_2$ states to the $^5I_8$ ground state. These emission lines confirm the incorporation of Ce^{3+} ions into the $Sr_4P_2O_7$ matrix and indicate that energy transfer processes and multiple electronic transitions are active. The presence of multiple sharp and intense peaks across the visible range suggests that $Sr_4P_2O_7:Ce^{3+}$ is capable of multicolor luminescence, making it suitable for optoelectronic and display applications.

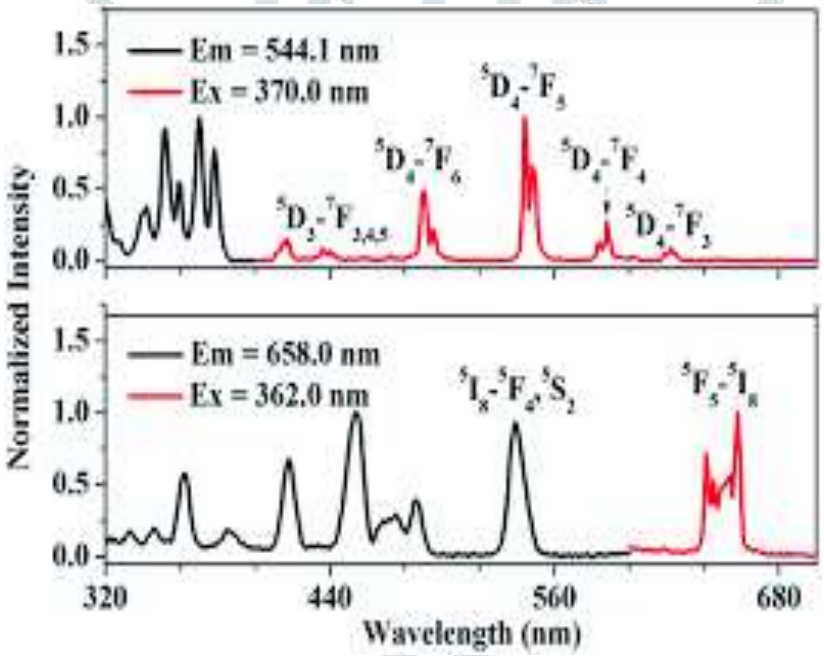

Figure 5: Photoluminescence (PL) of $Sr_4P_2O_7:Ce^{3+}$

Photoluminescence (PL) of $Sr_4P_2O_7:Dy^{3+}$

The photoluminescence (PL) spectra of $Sr_4P_2O_7:Dy^{3+}$ reveal characteristic excitation and emission behaviors of Dy^{3+} ions within the host matrix. The excitation spectrum (blue curve), monitored at an emission wavelength of 490 nm, displays multiple sharp peaks attributed to transitions from the ground state $^6H_{15/2}$ to various higher energy states such as $^4M_{15/2}$, $^6P_{7/2}$, $^6P_{3/2}$, and $^6I_{11/2}$, with a prominent peak observed around 353 nm, suggesting strong absorption in the near-UV region. The corresponding emission spectrum (red curve), recorded under 353 nm excitation, exhibits intense and well-resolved peaks centered at ~490 nm, ~575 nm, and ~660 nm. These peaks correspond to the $^4F_{9/2} \rightarrow {}^6H_{15/2}$ (blue emission), $^4F_{9/2} \rightarrow {}^6H_{13/2}$ (yellow emission), and $^4F_{9/2} \rightarrow {}^6H_{11/2}$ (red emission) transitions, respectively. The dominant yellow emission suggests potential applications of $Sr_4P_2O_7:Dy^{3+}$ in white-light-emitting devices, where Dy^{3+} acts as an efficient activator for generating multicolor luminescence from a single dopant.

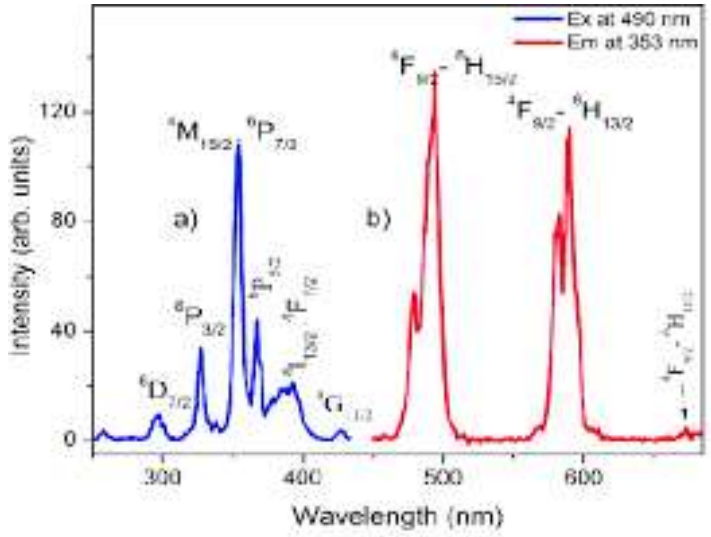

Figure 6: Photoluminescence (PL) of $Sr_4P_2O_7:Dy^{3+}$

III.Conclusion

The present study comprehensively investigated the photoluminescence (PL) properties of Ce^{3+}, Eu^{3+}, and Dy^{3+} doped phosphate-based nanophosphors using $Mg_4P_2O_7$, $Ca_4P_2O_7$, and $Sr_4P_2O_7$ as host lattices. These phosphors were successfully synthesized through a conventional high-temperature solid-state method, and their structural, morphological, and vibrational properties were confirmed using XRD, SEM, TEM, FT-IR, and TGA analyses. The incorporation of rare-earth ions into the phosphate lattices led to significant modifications in their optical characteristics, revealing intense and sharp emission lines upon UV excitation.

Among the phosphors studied, Eu^{3+}-doped $Mg_4P_2O_7$ and $Sr_4P_2O_7$ showed dominant red emissions centered around 615 nm and 612 nm, respectively, which are attributed to the $^5D_0 \rightarrow {}^7F_2$ electric dipole transition of Eu^{3+} ions. These sharp emissions indicate that Eu^{3+} ions occupy non-centrosymmetric sites in the host matrix, making these phosphors highly suitable for red components in white-light-emitting diodes (w-LEDs). Ce^{3+}-doped phosphors, on the other hand, exhibited broad green emission bands around 545 nm due to allowed 4f–5d transitions, which are desirable for display and UV-excited lighting applications.

The Dy^{3+}-doped $Sr_4P_2O_7$ phosphor displayed a combination of blue (~490 nm), yellow (~575 nm), and red (~660 nm) emissions, arising from the $^4F_{9/2} \rightarrow {}^6H_{15/2}$, $^4F_{9/2} \rightarrow {}^6H_{13/2}$, and $^4F_{9/2} \rightarrow {}^6H_{11/2}$ transitions, respectively. This multicolor emission behavior demonstrates the potential of Dy^{3+} ions to serve as single-dopant systems for generating near-white or tunable light. Additionally, the presence of both Eu^{2+} and Eu^{3+} emission bands in $Ca_4P_2O_7$ suggests partial reduction during synthesis and highlights the role of the host environment and synthesis conditions in determining the valence state and emission behavior.

A concentration-dependent study revealed that luminescence intensity initially increases with dopant concentration and reaches an optimum point, beyond which concentration quenching occurs due to non-radiative energy transfers and cross-relaxation processes among dopant ions. The optimal doping levels thus ensure maximum emission efficiency without detrimental effects.

Overall, the study demonstrates that rare-earth doped phosphate-based nanophosphors exhibit excellent luminescent performance with tunable emission colors, high crystallinity, and strong absorption in the UV region. These materials hold great promise for next-generation optoelectronic applications such as solid-state lighting, display panels, and UV-excited luminescent devices. Further research focusing on co-doping strategies, surface modifications, and controlled synthesis atmospheres could unlock enhanced performance and broader utility of these materials in photonic technologies.

References

1. Zhang, F. and Zhang, F., 2015. General introduction to upconversion luminescence materials. *Photon Upconversion Nanomaterials*, pp.1-20.
2. Klick, C.C. and Schulman, J.H., 1957. Luminescence in solids. In *Solid state physics* (Vol. 5, pp. 97-172). Academic Press.
3. Sławiński, J., 1988. Luminescence research and its relation to ultraweak cell radiation. *Experientia*, *44*(7), pp.559-571.
4. Steier, L., Poli de Figueiredo, J.A., Blatz, M.B. and Figueiredo, J.A.P.D., 2021. Fluorescence-Enhanced Theragnosis: A Novel Approach to Visualize, Detect, and Remove Caries. *Compendium of Continuing Education in Dentistry (15488578)*, *42*(8).
5. Cai, D.G., Zheng, T.F., Liu, S.J. and Wen, H.R., 2024. Fluorescence sensing and device fabrication with luminescent metal–organic frameworks. *Dalton Transactions*, *53*(2), pp.394-409.
6. Wu, N., Bo, C. and Guo, S., 2024. Luminescent Ln-MOFs for chemical sensing application on biomolecules. *ACS sensors*, *9*(9), pp.4402-4424.
7. Guo, X., Zhou, L., Liu, X., Tan, G., Yuan, F., Nezamzadeh-Ejhieh, A., Qi, N., Liu, J. and Peng, Y., 2023. Fluorescence detection platform of metal-organic frameworks for biomarkers. *Colloids and Surfaces B: Biointerfaces*, *229*, p.113455.

8. Yang, M., Guo, X., Mou, F. and Guan, J., 2022. Lighting up micro-/nanorobots with fluorescence. *Chemical Reviews*, *123*(7), pp.3944-3975.
9. Shu, Y., Ye, Q., Dai, T., Xu, Q. and Hu, X., 2021. Encapsulation of luminescent guests to construct luminescent metal–organic frameworks for chemical sensing. *ACS sensors*, *6*(3), pp.641-658.
10. Wang, H., Ai, L., Song, H., Song, Z., Yong, X., Qu, S. and Lu, S., 2023. Innovations in the solid-state fluorescence of carbon dots: strategies, optical manipulations, and applications. *Advanced Functional Materials*, *33*(41), p.2303756.
11. Liu, H., Shen, H., Zhang, H. and Wang, X., 2022. Development of photoluminescence phase-change microcapsules for comfort thermal regulation and fluorescent recognition applications in advanced textiles. *Journal of Energy Storage*, *49*, p.104158.
12. Zhang, R., Zhu, L. and Yue, B., 2023. Luminescent properties and recent progress in applications of lanthanide metal-organic frameworks. *Chinese Chemical Letters*, *34*(2), p.108009.
13. Wang, X. and Liu, W., 2024. A novel 2D Eu-MOF as a dual-functional fluorescence sensor for detection of benzaldehyde and Fe 3+. *Dalton Transactions*, *53*(28), pp.11850-11857.
14. Ansari, A.A., Thakur, V.K. and Chen, G., 2021. Functionalized upconversion nanoparticles: New strategy towards FRET-based luminescence bio-sensing. *Coordination Chemistry Reviews*, *436*, p.213821.
15. Chávez, D., Garcia, C.R., Oliva, J. and Diaz-Torres, L.A., 2021. A review of phosphorescent and fluorescent phosphors for fingerprint detection. *Ceramics International*, *47*(1), pp.10-41.
16. Corsini, F., Tatsi, E., Colombo, A., Dragonetti, C., Botta, C., Turri, S. and Griffini, G., 2021. Highly emissive fluorescent silica-based core/shell nanoparticles for efficient and stable luminescent solar concentrators. *Nano Energy*, *80*, p.105551.
17. Duman, F.D. and Forgan, R.S., 2021. Applications of nanoscale metal–organic frameworks as imaging agents in biology and medicine. *Journal of Materials Chemistry B*, *9*(16), pp.3423-3449.
18. Xu, C., Nedergaard, M., Fowell, D.J., Friedl, P. and Ji, N., 2024. Multiphoton fluorescence microscopy for in vivo imaging. *Cell*, *187*(17), pp.4458-4487.
19. Park, J., Park, B., Kim, T.Y., Jung, S., Choi, W.J., Ahn, J., Yoon, D.H., Kim, J., Jeon, S., Lee, D. and Yong, U., 2021. Quadruple ultrasound, photoacoustic, optical coherence, and fluorescence fusion imaging with a transparent ultrasound transducer. *Proceedings of the National Academy of Sciences*, *118*(11), p.e1920879118.
20. Mukunda, D.C., Joshi, V.K. and Mahato, K.K., 2022. Light emitting diodes (LEDs) in fluorescence-based analytical applications: A review. *Applied Spectroscopy Reviews*, *57*(1), pp.1-38.
21. Viana, L.N., Soares, A.P.S., Guimarães, D.L., Rojano, W.J.S. and Saint'Pierre, T.D., 2022. Fluorescent lamps: A review on environmental concerns and current recycling perspectives highlighting Hg and rare earth elements. *Journal of Environmental Chemical Engineering*, *10*(6), p.108915.
22. Yu, D., Zha, Y., Zhong, Z., Ruan, Y., Li, Z., Sun, L. and Hou, S., 2021. Improved detection of reactive oxygen species by DCFH-DA: New insight into self-amplification of fluorescence signal by light irradiation. *Sensors and Actuators B: Chemical*, *339*, p.129878.
23. Zhang, P. and Sun, X., 2024. Advanced multicolor dynamic fluorescence anti-counterfeiting and encryption strategy based on light-induced reversible perovskite lattice distortion. *Chemical Engineering Journal*, *498*, p.155658.
24. Suo, H., Zhu, Q., Zhang, X., Chen, B., Chen, J. and Wang, F., 2021. High-security anti-counterfeiting through upconversion luminescence. *Materials Today Physics*, *21*, p.100520.